Nanoscale

PAPER

View Article Online
View Journal | View Issue

Cite this: *Nanoscale*, 2025, **17**, 9534

Tuning infrared emissivity of multilayer graphene using ionic liquid gel electrolytes†

Ying Cao,‡[a] Kaiyu Yang,‡[a] Haibo Ke,[a] Lishi Fu,[a] Xitong Yan,[a] Jinghuan Xian,[a] Mingyuan Lin,[a] Weiwei Cai,[a] Xue-ao Zhang,[a,b] Rui Mu *[c] and Yufeng Zhang *[a,b]

Actively controlling the infrared (IR) emissivity of materials is critical for numerous applications, such as radiative cooling and thermal camouflage. Multilayer graphene (MLG) has shown significant potential as a functional material with tunable IR emissivity. However, the poor long-term stability of currently reported MLG-based IR modulators greatly limits their practical applications. Herein, ionic liquid gel electrolytes (ILGPEs) are prepared and used as doping sources to assemble MLG-based IR modulators with a sandwich-like structure. The modulator lifetime is dramatically improved, while the modulation depth and dynamic response are retained at levels comparable to those using pure ionic liquids. Microscopic structural analyses, including Raman spectroscopy and X-ray diffraction, are correlated with the ionic conductivity of the ILGPE and the IR radiation of the MLG. The results indicate that the improvement in device performance is likely due to an improved interface between the ILGPE and MLG, as well as limited ion diffusion within the ILGPE, which preserves the structural integrity of the MLG. These findings shed light on the optimization of IR modulators based on ion intercalation.

Received 22nd January 2025,
Accepted 19th March 2025

DOI: 10.1039/d5nr00322a

rsc.li/nanoscale

Introduction

According to the Stefan–Boltzmann law, a material's radiative energy can be modulated by altering either its surface temperature or emissivity. Compared to changing the surface temperature, modifying emissivity offers greater flexibility, efficiency, and robustness.[1,2] Consequently, the reversible adjustment of infrared (IR) emissivity holds significant importance for various applications, such as thermal management,[3–5] radiative cooling,[6–8] and thermal camouflage.[9–11]

Recent advances in adaptive thermal camouflage have spurred interest in materials capable of responding to various external stimuli. These include thermally induced phase change materials,[12,13] mechanically driven elastomeric materials,[14] electrochromic materials,[15,16] and wettability-modulated materials.[17] Furthermore, combining functional materials with optical designs (*e.g.*, tandem VO_2-based Fabry–Pérot cavities[18]) or introducing dopants (*e.g.*, W–Mg co-doping of VO_2[19]) enables multispectral and temperature-adaptive emissivity modulation. Nevertheless, among these materials, graphene stands out as a promising candidate for IR emissivity modulation, due to its linear dispersive energy band structure, excellent conductivity, and flexibility.[20–22] It has been shown that the Fermi level of graphene can be easily shifted by controlling the carrier concentration (*e.g.*, through electrostatic gating) with ionic liquids (ILs) serving as effective doping sources.[23] While it is known that such shift effectively changes graphene's optical band gap and IR emissivity, researchers have further studied emissivity modulators with varying back electrodes,[22,24,25] investigated the effects of different ILs on emissivity tuning,[26] demonstrated non-volatile and reversible tunability from visible to microwave wavelengths,[27] achieved continuous IR emissivity modulation using pulsed voltages,[28] and examined various factors, such as the number of graphene layers,[1] surface morphology[29] and long-term stability.[2]

While these studies highlight the promise of ILs for graphene-based IR modulators, they also reveal a critical

[a]College of Physical Science and Technology, Xiamen University, Xiamen 361005, China. E-mail: yufengzhang@xmu.edu.cn
[b]Jiujiang Research Institute of Xiamen University, Jiujiang, 360404, China
[c]School of Aerospace Engineering, Xiamen University, Xiamen 361102, China. E-mail: murui@xmu.edu.cn

† Electronic supplementary information (ESI) available: Comparison of gel polymers; optical images of ILGPE; thermal image of modulator without a celgard separator; thermal stability of ILGPE; electrochemical stability of ILGPE; dynamic modulation of MLG IR emissivity with different ILGPE concentrations; ionic conductivity of ILGPE; change in crystal structure of ILGPEs; completed cyclic test of MLG with an ILGPE concentration of 6; cyclic test of MLG with different ILGPE concentrations; performance of IR modulator with pure [AMIM]NTf_2 and ILGPE prepared using [AMIM]NTf_2; electrochemical impedance of ILGPE at different temperatures; SEM of MLG before and after ion intercalation; XRD of MLG before and after ion intercalation. See DOI: https://doi.org/10.1039/d5nr00322a

‡ These authors contribute equally.

challenge: the short lifespan of ion-intercalated graphene due to structural damage caused by the high diffusivity of pure ILs.[23,24,26–28] It has been reported that altering the structure of host materials (*e.g.*, replacing MLG with a graphene aerogel) could increase the modulator lifetime.[30] However, changing the host materials introduces other issues (*e.g.*, spatial inhomogeneity). Meanwhile, modifying the properties of guest materials (*e.g.*, introducing molecular components into ILs) offers an alternative approach to improve the performance of related devices.[31]

It has been demonstrated that ionic liquid gel electrolytes (ILGPEs), a hybrid of ILs and solid polymers, offer enhanced safety, thermal stability, and electrode/electrolyte interface performance, compared to their liquid and solid counterparts.[32–35] Common gel polymers include polyvinyl alcohol (PVA), polymethyl methacrylate (PMMA), polyvinylidene fluoride (PVDF), and polyvinylidene fluoride-hexafluoropropylene copolymer (PVDF-HFP).[36–39] Some key parameters of ILGPEs prepared using different gel polymers are shown in ESI S1.† Generally, ILGPEs prepared with PVDF and PVDF-HFP exhibit higher ionic conductivity and a wider electrochemical stability window (ESW) than those using PVA and PMMA,[40,41] likely due to the presence of a fluorinated structure. Furthermore, PVDF-HFP provides better thermal stability than the other polymers, while HFP reduces the reactivity of F^-, which enhances liquid electrolyte retention and improves the interface stability between the electrode and electrolyte.[37] It has been proven that ILGPEs effectively improve performance for batteries.[32,33,37] However, there are few reports investigating the application of ILGPE in IR modulators.

In this study, ILGPEs are synthesized using PVDF-HFP and two ionic liquids, namely 1-hexyl-3-methylimidazolium bis[(trifluoromethyl)sulfonyl]imide ([HMIM]NTf_2) as well as 1-allyl-3-methylimidazolium bis[(trifluoromethyl)sulfonyl]imide ([AMIM]NTf_2). The prepared ILGPEs are utilized to assemble IR modulators, which tune the emissivity of multilayer graphene (MLG) through electrostatic gating. The experimental characterizations (*e.g.*, Raman spectroscopy, X-ray diffraction and thermal imaging) reveal the effects of IL concentration on the modulator performance (*e.g.*, device stability). The results show that the modulator lifetime can be significantly improved, while the modulation depth and dynamic response are maintained, by replacing IL with ILGPE in the modulators.

Experimental section

Preparation of MLG

The MLG deposited on nickel by chemical vapor deposition (purchased from Changzhou Zooxi Electronic Technology Co., Ltd) was etched in an 8% ferric chloride solution for 12 hours to remove the nickel. Then, the etched MLG was washed repeatedly with deionized water. Finally, the MLG was collected using a Celgard 2325 separator (25 μm thick, polypropylene–polyethylene–polypropylene, Celgard Inc.) and dried in an oven at 60 °C.

Preparation of ILGPE

The ILGPEs were prepared by mixing ILs (either [HMIM]NTf_2 or [AMIM]NTf_2, from Lanzhou Institute of Chemical Physics, China.) with PVDF-HFP (Guangdong Wengjiang Chemical Reagent Co., Ltd, China) and *N*,*N*-dimethylformamide (DMF) (Shanghai Jizhi Biochemical Technology Co., Ltd, China, with a purity of 99%). The masses of PVDF-HFP and DMF were kept constant (*i.e.*, 0.2 g and 2.0 g, respectively), while the mass of ILs was varied from 0.8 to 1.6 g to prepare ILGPEs with different concentrations. In this paper, the concentration of the ILGPE is defined as the mass ratio of IL to PVDF-HFP. For example, the ILGPE with a concentration of 6 was prepared using 1.2 g ILs. The mixture was magnetically stirred at 1000 rpm for 2 hours. Finally, the solution was cast into a polytetrafluoroethylene (PTFE) mold and placed in an oven at 80 °C for 6 hours. As shown in ESI S2,† the prepared ILGPE is flexible and transparent. Note that, unless otherwise specified, ILGPE refers to the gel polymer electrolyte made using [HMIM]NTf_2.

Device assembly

MLG (supported on a Celgard separator) and metal copper foil (99%, Alfa Aesar Inc.) served as the top (positive) and back (negative) electrodes, respectively. The ILGPE was placed in between to provide an ionic intercalation source for the MLG-based IR modulator.

Thermal imaging

Thermal images and videos were recorded *in situ* using an infrared camera (A655sc, Teledyne FLIR, USA) with a spectral range of 7.5–14 μm. The ambient temperature (T_0) and the real temperature of the modulator (T_R) were measured using thermocouples. Voltage was applied to the MLG-based modulator using an electrochemical workstation (CHI660E, Shanghai Chenhua Instruments Co., Ltd, China).

Sample characterization

The morphology of the MLG films was investigated using scanning electron microscopy (SEM, Carl Zeiss FE-SEM Sigma HD). The crystal structure of MLG before and after ion intercalation was characterized by X-ray diffraction (XRD, MAXima XRD-7000) with a Cu K_α excitation source and Raman spectroscopy (WITec alpha 300 RA) with 488 nm line of an Ar^+ laser at room temperature. The thermal stability of ILGPEs was determined using a thermogravimetric analyzer (Mettler Toledo TGA2). The ESW was characterized by linear sweep voltammetry (LSV) at a scan rate of 1 mV s^{-1}, while the conductivity of ILGPEs was determined by electrochemical impedance spectroscopy (EIS) using the electrochemical workstation.

Results and discussion

Fig. 1(a) depicts the structure of the sandwich-like modulator and the setup for thermal imaging. The modulator consists of four layers: back electrode (*i.e.*, the metal copper foil), ILGPE

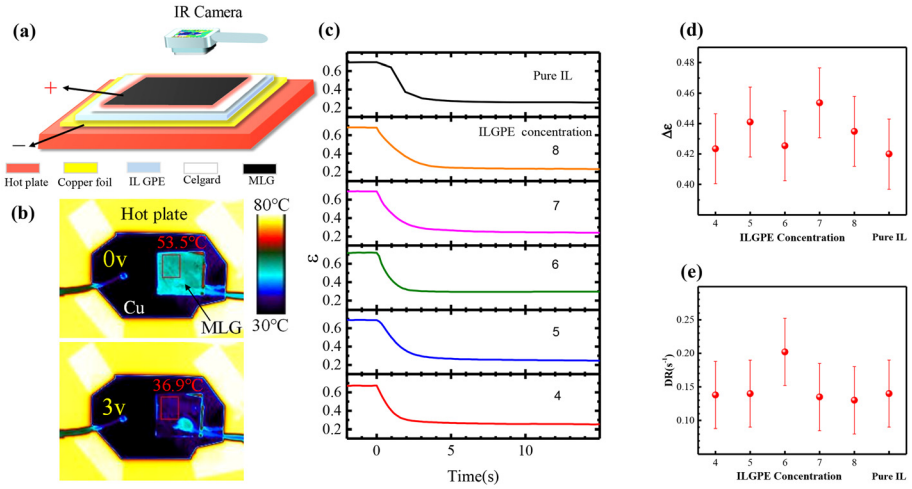

Fig. 1 Structure and performance of the MLG-based IR modulator. (a) Schematic diagram of the modulator; (b) thermal images of the modulator before and after applying a bias voltage; (c) the emissivity of MLG as a function of time, when different concentrations of ILGPEs are used as the doping sources; (d) modulation depth and (e) dynamic response of the modulator plotted against the ILGPE concentration, with the results of pure IL as references.

as the ion source, Celgard separator, and front electrode (*i.e.*, MLG). Note that copper foil is commonly used as the back electrode in an emissivity modulator,[24,42] because it provides good electrical conductivity (ensuring efficient charge transport) and possesses low emissivity (minimizing interference with the MLG emissivity measurement). Furthermore, copper is significantly cheaper than noble metals like gold, making it an attractive option for large-scale fabrication. Meanwhile, the modulator without a Celgard separator exhibits similar performance (*e.g.*, modulation depth) to that with Celgard, as shown in ESI S3,† since ILGPE can function as a separator in the modulator to prevent short-circuiting. However, it remains challenging to directly transfer an intact MLG onto ILGPE. Hence, in this study, the Celgard separator is retained to facilitate easier modulator fabrication (*i.e.*, providing physical support for MLG).

The modulator sits on a hotplate set to a temperature of 70 °C during the study. Note that the ILGPE is thermally stable at this temperature, as evidenced by thermogravimetric analyses shown in ESI S4,† where no obvious mass loss or decomposition occurs before reaching 380 °C. The bias voltage is applied to the device using the electrochemical workstation, while the current is recorded during the ion insertion and extraction processes. The thermal images are recorded *in situ*, from which the apparent temperature of the modulator (T_{IR}) is extracted.

Fig. 1(b) shows representative thermal images of the modulator. After applying a bias voltage of 3 V, the color of MLG uniformly changes from green to blue, indicating a decrease in T_{IR}. Note that the yellowish and bluish colors represent high and low T_{IR}, respectively. It is worth noting that the ILGPE is electrochemically stable at this voltage, as evidenced by LSV shown in ESI S5.†

Further analysis shows that the average T_{IR} in the rectangular region drops from 53.5 °C to 36.9 °C, after applying the bias voltage. This indicates that the emissivity of MLG can be adjusted from the high state to the low state using ILGPE as the doping source. The dynamic modulation of the MLG thermal radiation is further illustrated in ESI Videos V1.†

In order to quantitatively analyze the changes in thermal radiation of the modulator, the infrared emissivity of MLG (ε) is calculated using the formula[23]

$$\varepsilon = \frac{{T_{IR}}^4 - {T_0}^4}{{T_R}^4 - {T_0}^4} \quad (1)$$

The uncertainty in the ε is estimated to be ±0.04. Fig. 1(c) shows the evolution of the ε over time t for different concentrations of ILGPE. A bias of +3 V is supplied at t = 0 s. Overall, ε decreases dramatically for all samples after applying the bias voltage. This exponential decrease in ε is likely due to the increased dopant concentration in the MLG during the charging process. Additional thermal images of the modulator with different ILGPE concentrations are provided in ESI S6.†

To quantitatively analyze the impact of ILGPE on the modulator performance, the modulation depth $\Delta\varepsilon$, defined as the difference between the maximum value of ε (ε_{max}) and the minimum value of ε (ε_{min}), is plotted against the ILGPE concentration, as shown in Fig. 1(d). Clearly, $\Delta\varepsilon$ remains roughly constant at 0.43 across different ILGPE concentrations, which is similar to the reported value of 0.42 for modulators using pure IL.[23,26] Hence, the ability to tune ε is retained when the doping source is switched from pure IL to ILGPE. Furthermore, it is observed that ILGPE concentrations below 4 are not effective for IR modulation, as the high polymer content leads to a low ionic conductivity and poor interface between the ILGPE and MLG, which prevents efficient ion transport.

Moreover, the dynamic response (D_R), another key property of the modulator is defined as:[31]

$$D_R = \frac{\varepsilon_{max} - \varepsilon_{min}}{\Delta t} \quad (2)$$

where Δt is the time required to reduce the modulator emissivity from ε_{max} to ε_{min}. The uncertainty of D_R is estimated to be $\pm 0.05\ s^{-1}$. Fig. 1(e) depicts the relationship between D_R and ILGPE concentration. Clearly, an optimal value is reached with a moderate ILGPE concentration. For example, when the ILGPE concentration is 6, the D_R reaches a maximum value of $0.25\ s^{-1}$, which is 2.5 times that of pure IL ($0.1\ s^{-1}$ (ref. 23 and 26)). Increasing the IL content leads to a higher ion concentration in the ILGPE, as evidenced by the increase in ionic conductivity of ILGPE with higher IL content, derived from the corresponding Nyquist plots, as shown in ESI S7.† Furthermore, the XRD analyses of ILGPEs, shown in ESI S8,† reveal that the amorphousness of the polymer matrix increases with increasing IL content. This creates more conduction sites for efficient ion transport,[43] thereby improving ionic conductivity. Nevertheless, with higher IL content, more charges can be transferred to the MLG in the same period of time under the same bias voltage, which facilitates a quicker reduction in ε. However, further increasing the IL content may lead to ion pairing or clustering,[44] as well as disrupt ion pathways in the gel electrolyte, thus causing a decrease in D_R and, in extreme cases, IL leakage similar to that observed in pure IL. Note that, when the ILGPE concentration exceeds 8, it becomes challenging to form a complete and continuous ILGPE.

Long-term stability (*i.e.*, modulator lifetime) is one of the most critical properties for practical application of modulators. Hence, the modulators were subjected to cyclic voltage testing, where a voltage of 3 V was applied for 10 s, followed by 0 V for 10 s. A selection of cycles from the cyclic test for the modulator with an ILGPE concentration of 6 is shown in Fig. 2(a), allowing for easy tracking of the change in modulation of ε. The variation in ε over the initial 500 s is shown in the inset of Fig. 2(a), whereas the complete cyclic test is depicted in the ESI S9.† Additionally, dynamic modulation of the MLG thermal radiation is further demonstrated in ESI Videos V2.† As expected, the ε changes between the high and low states with the application of the bias voltage. Interestingly, the value of ε in the high state decreases with increasing cycle number, while the value in the low state decreases initially, but gradually increases after approximately 1000 cycles. The $\Delta\varepsilon$ for each cycle shown in Fig. 2(a) is calculated and plotted in Fig. 2(b). Clearly, the modulator operates stably for up to around 1000 cycles, which corresponds to approximately 6 hours. However, the modulator performance degrades dramatically beyond this point. The $\Delta\varepsilon$ for modulators with other ILGPE concentrations in the cyclic tests are shown in ESI S10.†

In this study, the modulator is considered inoperable when the $\Delta\varepsilon$ falls below 0.1. At this circumstance, the difference in thermal images of the modulator before and after applying the bias voltage becomes negligible. The lifetime for modulator with varying ILGPE concentrations is shown in Fig. 2(c). For the modulator using pure IL, the modulator lifetime is around 50 cycles, which is slightly lower than the previously reported value of 160 cycles[24] (as indicated by the blue point in Fig. 2(c)). The deviation may be attributed to the difference in the applied voltage. The literature uses a bias of 2.75 V, while this study uses a higher voltage of 3 V. The higher voltage may accelerate ionic intercalation into MLG, potentially causing more structural damage. Nevertheless, the modulator lifetime increases greatly to over 600 cycles when ILGPE is used as the doping source. A similar improvement in modulator lifetime is also observed for the ILGPE prepared using [AMIM]NTf_2, as shown in ESI S11.† This suggests that the strategy of improving modulator stability by replacing pure IL with ILGPE is applicable to other ILs.

Generally, the short lifetime of emissivity modulators using pure ILs is due to several factors: oxidation defects on MLG caused by air exposure at elevated temperatures,[45] side reactions between MLG and ions in ILs,[2] and intercalation-induced structural damage (*e.g.*, increased interlayer spacing, weakened van der Waals forces between graphene layers).[26,30] These factors result in structural distortions (*e.g.*, swelling, delamination) and, in extreme cases, IL leakage, which greatly degrade modulator performance. Unlike pure IL, ILGPE incorporates a polymer matrix that plays a crucial role in improving the stability of the IR modulator. The polymer network physically retains the ionic liquid, preventing leakage while also limiting direct contact between reactive species and the electrode (MLG) surface.[46] This minimizes unwanted side reactions at the electrode. Additionally, the ILGPE formulation

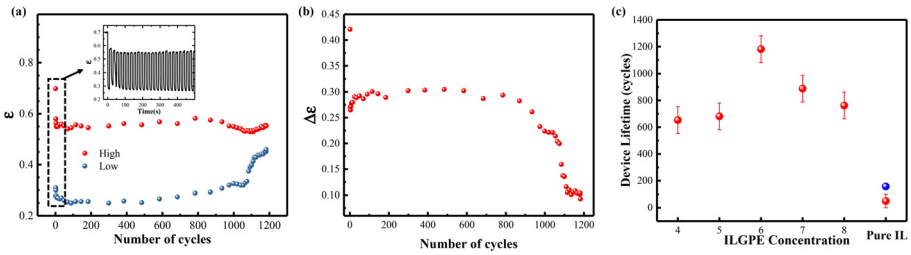

Fig. 2 Long-term stability of the modulator. (a) Cyclic test of the MLG-based IR modulator with an ILGPE concentration of 6, with the inset demonstrating the emissivity of MLG changing over time during the initial 500 s; (b) evolution of modulation depth as a function of cycle number; (c) correlation between modulator lifetime and ILGPE concentration.

enables controlled ion mobility, reducing excessive ionic redistribution that could otherwise lead to performance degradation. Therefore, replacing IL with ILGPE improves modulator stability.

Furthermore, there is an optimal ILGPE concentration for achieving the maximum modulator lifetime. In this study, the maximum lifetime (*i.e.*, 1100 cycles, approximately 7 times that of pure IL) is observed at an ILGPE concentration of 6. As demonstrated in other studies, chemical reactions between IL and MLG as well as intercalation-induced structural damage of MLG, contribute to a reduced modulator lifetime.[2,26,47] By limiting the amount of IL in the ILGPE, the modulator lifetime can be extended. However, a low IL content (*i.e.*, high polymer content) may reduce the ESW[41] and lead to poor interfacial contact between the ILGPE and MLG, which increases interfacial resistance and uneven current distribution, in turn accelerating degradation processes.[48] This is also evident from the inability to fabricate a functional modulator with an ILGPE concentration lower than 4. Meanwhile, other factors, such as increasing internal resistance due to low ionic conductivity and the higher risk of side reactions due to a narrower ESW, may contribute to a reduced modulator lifetime when the ILGPE concentration is too low.[49] On the other hand, as discussed in the relationship between ILGPE concentration and dynamic response, excessive IL content can reduce modulator lifetime by compromising the structure of the gel polymer electrolyte and MLG.

To better understand the ion transport in ILGPE, the EIS of ILGPE with a concentration of 6 is measured at different temperatures. In the high-frequency region of the Nyquist plot, as shown in ESI S12,† the intercept of the curve with the real axis (Z') corresponds to the intrinsic resistance of the ILGPE (R). The ionic conductivity (σ) of ILGPE was calculated using the formula[37]

$$\sigma = \frac{L}{S \cdot R} \tag{3}$$

where L is the thickness of the ILGPE, and S is the geometric area of the electrode/electrolyte interface. The logarithm of σ ($\log \sigma$) is approximately inversely proportional to temperature, as shown in Fig. 3(a). This relationship fits well with the typical Arrhenius model, as suggested in many studies.[37,50–52] Hence, the ion mobility of ILGPE is lower than that of pure IL, especially at low temperatures. As suggested by previous studies,[26] rapid ion transport may compromise the structural integrity of the electrode (*i.e.*, MLG). Hence, reducing ion mobility helps to improve the modulator lifetime.

To further confirm the mechanism underlying the improved performance of the modulator, MLG samples were extracted from the modulators after applying a bias voltage and investigated using SEM and Raman spectroscopy. The SEM images, shown in ESI S13,† reveal that fewer defects are present in the MLGs using ILGPE as the doping source, compared to those using pure IL. To better understand the changes in the microscopic structure of MLG, Raman spectra of MLG extracted from failed modulators with different concentrations of ILGPE are shown in Fig. 3(b), with the spectra of pristine MLG and MLG with pure IL used as references. The features around 1355 cm^{-1} and 1585 cm^{-1} are assigned to the D and G bands of MLG, respectively. The D band is associated with defects or impurities in graphene,[53] while the G band corresponds to the zone-center vibration of carbon atoms within the graphene planes.[54] The spectrum of pristine MLG exhibits a sharp G band with a negligible D band, which rep-

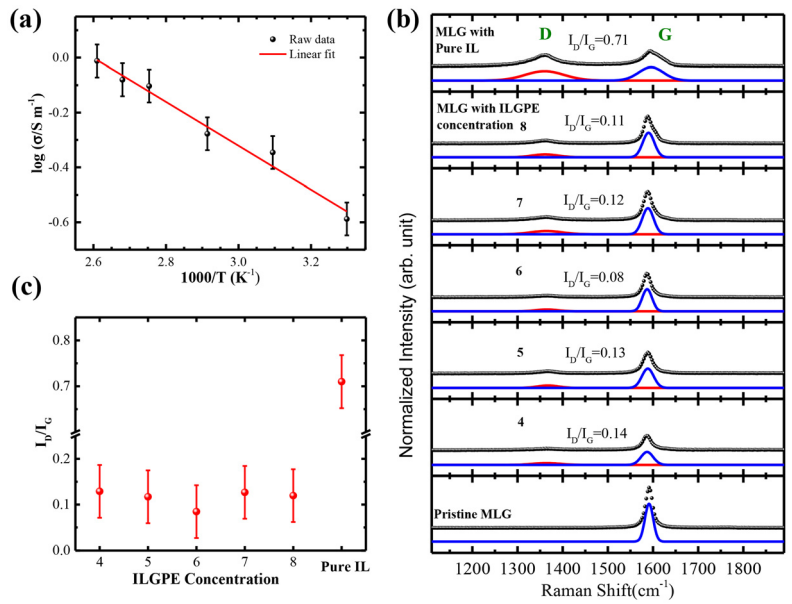

Fig. 3 (a) Ionic conductivity of ILGPE with a concentration of 6 as a function of temperature; (b) Raman spectra and fitted curves of MLG extracted from the modulators after their failure; (c) the I_D/I_G ratio as a function of ILGPE concentration.

resents high-quality graphene. However, an observable D band appears in all spectra of MLG extracted from the failed modulators. This confirms that the structure of MLG is compromised after extensive ion intercalation. Furthermore, the degradation of the structural integrity of MLG is further evidenced by changes in XRD patterns shown in ESI S14.† The intensity of the MLG (002) peak at 26.5° decreases with an increasing number of cycles. This suggests that the stacking structure of graphene layers in MLG is gradually disrupted due to the insertion of ions (*e.g.*, $[NTf_2]^-$).

Moreover, the D band is more prominent in the MLG with pure IL, compared to the MLG with ILGPE. To quantitatively evaluate the defect density in MLG, the Raman spectra are fitted using multiple Voigt functions, as shown in Fig. 3(b). The intensity ratio of the D band to the G band (I_D/I_G) is derived and used as an indicator for the defect density of MLG.[26] The I_D/I_G is plotted against the ILGPE concentration, as shown in Fig. 3(c). Clearly, the I_D/I_G values for MLGs with ILGPE are significantly smaller than those of MLG with pure IL. Therefore, replacing pure IL with ILGPE effectively reduces the defect density in MLG, induced by ion intercalation. This contributes to the improvement of modulator lifetime, which is consistent with the results shown in Fig. 2(c). For instance, the I_D/I_G value reaches a minimum at an ILGPE concentration of 6, which aligns with the maximum modulator lifetime.

Conclusion

In this study, ILGPEs with different IL content, prepared using ionic liquids ([HMIM]NTf_2 and [AMIM]NTf_2) and PVDF-HFP, are deployed as doping sources for regulating the IR emissivity of MLG through electrostatic gating. The modulator lifetime of the MLG-based IR modulator is dramatically improved, while the modulation depth and dynamic response are maintained. It is found that a moderate amount of IL (*i.e.*, the ILGPE with a concentration of 6) offers the best results, likely due to an optimal balance between ionic conductivity and interfacial properties of the ILGPE. Microscopic structure analyses of MLG, revealed by Raman spectroscopy and XRD, suggest that the enhancement in long-term stability is attributed to better preservation of the structural integrity of MLG, when ILGPE is used, compared to pure IL. This is due to the limited free diffusion of IL in the ILGPE, which in turn results in less damage to the MLG structure caused by ion intercalation. These results pave a novel avenue for optimizing IR modulators based on ion intercalation, which holds great potential for applications in thermal management and adaptive camouflage.

Author contributions

Y. C. prepared and characterized the modulator. K. Y. performed the data analysis. H. K., L. F., X. Y., J. X., M. L. and W. C. support the investigation. R. M. verified the results and edited the manuscript. X. Z. administrated the project, and Y. Z. conceived the idea and supervised the project. All the authors participated in discussions of the research, and have given approval to the final version of the manuscript. Y. C. and K. Y. contribute equally to this study.

Data availability

The data supporting this article have been included as part of ESI.†

Conflicts of interest

The authors declare no conflicts of interest.

Acknowledgements

This study was financially supported by the National Natural Science Foundation of China (No. 12174321 and 12374193).

References

1 P. Ding, P. Wang, J. Su, B. Mao, M. Ren, K. Xu, S. Tian, Y. Li, X. Tian and J. Wang, *J. Phys. D: Appl. Phys.*, 2022, **55**, 345103.
2 X. Yu, G. Bakan, H. Guo, M. S. Ergoktas, P. Steiner and C. Kocabas, *ACS Nano*, 2023, **17**, 11583–11592.
3 Y. Yang, X. Zhou, X. Ji, W. Liu, Q. Li, C. Zhu, X. Li, S. Liu, X. Lu and J. Qu, *Adv. Funct. Mater.*, 2025, **35**, 2416776.
4 Z. Yan, H. Zhai, D. Fan and Q. Li, *Nano Today*, 2023, **51**, 101897.
5 H. Ni, X. Zhang, J. Yu, C. Zhao and Y. Si, *ACS Appl. Mater. Interfaces*, 2024, **16**, 62654–62663.
6 B. Wang, L. Li, H. Liu, T. Wang, K. Zhang, X. Wu and K. Yu, *Sol. Energy Mater. Sol. Cells*, 2025, **280**, 113291.
7 J. Xu, X. Wu, Y. Li, S. Zhao, F. Lan, A. Xi, Y. Huang, Y. Ding and R. Zhang, *Nano Lett.*, 2024, **24**, 15178–15185.
8 Y. Jung and S. H. Ko, *iScience*, 2024, **27**, 111325.
9 H. Zhu, Q. Li, C. Zheng, Y. Hong, Z. Xu, H. Wang, W. Shen, S. Kaur, P. Ghosh and M. Qiu, *Light: Sci. Appl.*, 2020, **9**, 60.
10 B.-X. Li, Z. Luo, W.-G. Yang, H. Sun, Y. Ding, Z.-Z. Yu and D. Yang, *ACS Nano*, 2023, **17**, 6875–6885.
11 B.-F. Guo, Y.-J. Wang, C.-F. Cao, Z.-H. Qu, J. Song, S.-N. Li, J.-F. Gao, P. Song, G.-D. Zhang, Y.-Q. Shi and L.-C. Tang, *Adv. Sci.*, 2024, **11**, 2309392.
12 Q. Kang, D. Li, K. Guo, J. Gao and Z. Guo, *Nanomaterials*, 2021, **11**, 260.
13 J. Lyu, Z. Liu, X. Wu, G. Li, D. Fang and X. Zhang, *ACS Nano*, 2019, **13**, 2236–2245.
14 H. Fang, W. Xie, X. Li, K. Fan, Y.-T. Lai, B. Sun, S. Bai, W. J. Padilla and P.-C. Hsu, *Nano Lett.*, 2021, **21**, 4106–4114.

15 J. Niu, Y. Wang, X. Zou, Y. Tan, C. Jia, X. Weng and L. Deng, *Appl. Mater. Today*, 2021, **24**, 101073.
16 G. Zeng, R. Zhang, Y. Tan, X. a. Cheng and T. Jiang, *ACS Photonics*, 2021, **8**, 3599–3606.
17 J. Mandal, M. Jia, A. Overvig, Y. Fu, E. Che, N. Yu and Y. Yang, *Joule*, 2019, **3**, 3088–3099.
18 H. Wei, J. Gu, T. Zhao, Z. Yan, H.-X. Xu, S. Dou, C.-W. Qiu and Y. Li, *Light: Sci. Appl.*, 2024, **13**, 54.
19 C. Geng, Y. Chen, H. Wei, T. Zhao, Q. Zhao, Z. Tian, S. Dou, Y. Liu and Y. Li, *Adv. Funct. Mater.*, 2024, **34**, 2410819.
20 H. Liu, Q. Ai and M. Xie, *Int. J. Therm. Sci.*, 2022, **171**, 107225.
21 A. H. Castro Neto, F. Guinea, N. M. R. Peres, K. S. Novoselov and A. K. Geim, *Rev. Mod. Phys.*, 2009, **81**, 109–162.
22 P. Avouris, *Nano Lett.*, 2010, **10**, 4285–4294.
23 O. Salihoglu, H. B. Uzlu, O. Yakar, S. Aas, O. Balci, N. Kakenov, S. Balci, S. Olcum, S. Süzer and C. Kocabas, *Nano Lett.*, 2018, **18**, 4541–4548.
24 Y. Sun, Y. Wang, C. Zhang, S. Chen, H. Chang, N. Guo, J. Liu, Y. Jia, L. Wang, Y. Weng, W. Zhao, K. Jiang and L. Xiao, *ACS Appl. Mater. Interfaces*, 2019, **11**, 13538–13544.
25 M. S. Ergoktas, G. Bakan, P. Steiner, C. Bartlam, Y. Malevich, E. Ozden-Yenigun, G. He, N. Karim, P. Cataldi, M. A. Bissett, I. A. Kinloch, K. S. Novoselov and C. Kocabas, *Nano Lett.*, 2020, **20**, 5346–5352.
26 H. Huang, J. Li, H. Ke, Y. Du, W. Peng, M. Dai, Y. Zhang and X.-a. Zhang, *ACS Appl. Mater. Interfaces*, 2021, **13**, 26256–26263.
27 M. S. Ergoktas, G. Bakan, E. Kovalska, L. W. Le Fevre, R. P. Fields, P. Steiner, X. Yu, O. Salihoglu, S. Balci, V. I. Fal'ko, K. S. Novoselov, R. A. W. Dryfe and C. Kocabas, *Nat. Photonics*, 2021, **15**, 493–498.
28 J. Li, W. Peng, H. Huang, H. Ke, Z. Liu, R. Huang, X. Guo, S. Cheng, Y. Zhang, M. Dai and X.-a. Zhang, *Appl. Phys. Lett.*, 2022, **121**, 042204.
29 J. Su, P. Ding, P. Wang, B. Mao, M. Ren, K. Xu, F. Zeng and J. Wang, *Diamond Relat. Mater.*, 2023, **135**, 109848.
30 Z. Weng, H. Ke, X. Guo, S. Cheng, T. Lin, W. Peng, M. Dai, W. Cai, Y. Zhang and X.-a. Zhang, *Phys. Rev. Appl.*, 2022, **18**, 034003.
31 Y. Zhang, H. Ke, J. Li, Z. Weng, T. Lin, W. Peng, M. Dai, R. Mu and X.-A. Zhang, *Appl. Phys. Lett.*, 2022, **120**, 243504.
32 X. Cheng, J. Pan, Y. Zhao, M. Liao and H. Peng, *Adv. Energy Mater.*, 2018, **8**, 1702184.
33 X. Yang, F. Zhang, L. Zhang, T. Zhang, Y. Huang and Y. Chen, *Adv. Funct. Mater.*, 2013, **23**, 3353–3360.
34 J. Wang, G. Chen and S. Song, *Electrochim. Acta*, 2020, **330**, 135322.
35 S. Wang, Y. Jiang and X. Hu, *Adv. Mater.*, 2022, **34**, 2200945.
36 J. P. Serra, R. S. Pinto, J. C. Barbosa, D. M. Correia, R. Gonçalves, M. M. Silva, S. Lanceros-Mendez and C. M. Costa, *Sustainable Mater. Technol.*, 2020, **25**, e00176.
37 R. Mishra, S. K. Singh, H. Gupta, R. K. Tiwari, D. Meghnani, A. Patel, A. Tiwari, V. K. Tiwari and R. K. Singh, *Energy Fuels*, 2021, **35**, 15153–15165.
38 Y. Lian, M. Li, Y. Gao, M. Zhao, J. Liu and L. Xiao, *ACS Appl. Energy Mater.*, 2023, **6**, 11364–11375.
39 S. Alipoori, S. Mazinani, S. H. Aboutalebi and F. Sharif, *J. Energy Storage*, 2020, **27**, 101072.
40 D. Kumar, *Solid State Ionics*, 2018, **318**, 65–70.
41 F. C. A. Silva, P. F. R. Ortega, R. A. dos Reis, R. L. Lavall and L. T. Costa, *Electrochim. Acta*, 2022, **427**, 140831.
42 L. Zhao, R. Zhang, C. Deng, Y. Peng and T. Jiang, *Nanomaterials*, 2019, **9**, 1096.
43 T. Sharma, B. Gultekin, P. S. Dhapola, N. G. Sahoo, S. Kumar, D. Agarwal, H. K. Jun, D. Singh, G. Nath, P. K. Singh and A. Singh, *J. Mol. Liq.*, 2022, **352**, 118494.
44 V. Madhani, D. Kumar, M. Patel, B. P. Patel, S. Aslam, K. Mishra and M. S. Rathore, *Ionics*, 2025, **31**, 525–539.
45 M. D. Bhatt, H. Kim and G. Kim, *RSC Adv.*, 2022, **12**, 21520–21547.
46 Z. Deng, Y. Liu and Z. Dai, *Chem. – Asian J.*, 2023, **18**, e202201160.
47 W. M. Dose, I. Temprano, J. P. Allen, E. Björklund, C. A. O'Keefe, W. Li, B. L. Mehdi, R. S. Weatherup, M. F. L. De Volder and C. P. Grey, *ACS Appl. Mater. Interfaces*, 2022, **14**, 13206–13222.
48 L. M. McGrath, J. Jones, E. Carey and J. F. Rohan, *ChemistryOpen*, 2019, **8**, 1429–1436.
49 F. Wu, G. Tan, R. Chen, L. Li, J. Xiang and Y. Zheng, *Adv. Mater.*, 2011, **23**, 5081–5085.
50 Z. Li, J. Fu, X. Zhou, S. Gui, L. Wei, H. Yang, H. Li and X. Guo, *Adv. Sci.*, 2023, **10**, 2201718.
51 M. Menisha, S. L. N. Senavirathna, K. Vignarooban, N. Iqbal, H. M. J. C. Pitawala and A. M. Kannan, *Solid State Ionics*, 2021, **371**, 115755.
52 J. Zheng, W. Li, X. Liu, J. Zhang, X. Feng and W. Chen, *Energy Environ. Mater.*, 2023, **6**, e12422.
53 A. C. Ferrari and D. M. Basko, *Nat. Nanotechnol.*, 2013, **8**, 235–246.
54 L. Bokobza, J.-L. Bruneel and M. Couzi, *Vib. Spectrosc.*, 2014, **74**, 57–63.

